Analysis of Envelope Signal Injection for Improvement of RF Amplifier Intermodulation Distortion

Vincent W. Leung, *Member, IEEE*, Junxiong Deng, *Student Member, IEEE*, Prasad S. Gudem, and Lawrence E. Larson, *Fellow, IEEE*

Abstract—Adaptive bias techniques based on envelope signal power detection have been proposed for linearity enhancement and dc current reduction in RF amplifiers. Experimental results show an improvement in amplifier linearity, although asymmetric intermodulation distortion (IMD) was observed. This work rigorously studies the effects of the envelope signal injection on amplifier distortion using the Volterra series formulations. The results intuitively explain the spectral regrowth asymmetry, and point to a design technique in which third-order IMD can be optimally cancelled. The theory was verified through comparison to measurement and simulation results.

Index Terms—Adaptive bias, BiCMOS integrated circuits, envelope injection, intermodulation distortion, RF amplifier, SiGe, spectral regrowth, Volterra Series, wideband code division multiple access (WCDMA).

I. INTRODUCTION

THIRD-GENERATION (3G) wireless communication promises to deliver high bandwidth data services to cellular phone users. Application examples include wireless picture sharing, video conferencing and internet access. To accommodate high data-rate transmission over a wireless channel, spectrally efficient variable envelope modulation schemes are employed. The hybrid phase-shift keying (HPSK) adopted for the wideband CDMA (WCDMA) standard is one example [1]. Spectral regrowth due to transmitter circuit distortion must be strictly limited; this often translates to stringent and challenging linearity requirements for the transmitter chain radio frequency (RF) amplifier circuits. For mobile terminals, the maximum allowable adjacent channel power ratio (ACPR) at 5 MHz and 10 MHz offsets are specified to be −33 and −43 dBc, respectively.

Another important, although often conflicting, design criterion is minimizing the amplifier power consumption. Since RF amplifiers consume a significant share of the battery power in
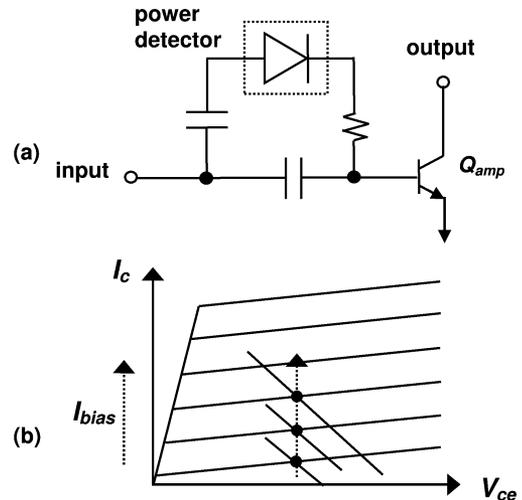
Fig. 1. (a) Conceptual diagram of the adaptively biased RF amplifier. (b) The power detector adjusts the amplifier loadline in response to increase in signal power.

a mobile device, their power efficiencies have a direct and determining impact on the talk time. Significant results on a high-linearity high-efficiency amplifier design employing optimum baseband termination were reported in [2].

Further complicating the issue, not only should the power efficiency be maximized at the peak power level (without compromising the amplifier linearity), it should also be kept high during the power backoff mode. It is because in, for instance, the WCDMA standard, power control is continuously enforced to equalize the signal strengths arriving at the basestation from multiple mobile devices to combat the "near-far" problem [3]. As a result, the amplifier circuit should exhibit high *average* efficiency to prolong battery life. This necessitates adaptive amplifier bias; for small-signal conditions, the quiescent current should be kept to its minimum to enhance the efficiency. For large-signal conditions, the current should automatically rise so that high linearity is achieved. This is effectively a "current on-demand" biasing scheme.

Various forms of adaptive-biased RF amplifiers were recently proposed [4]–[6]. The underlying concept is illustrated in Fig. 1(a). An envelope-tracking detector circuit (as denoted by the diode device) senses the average signal power and adjusts the amplifier bias level accordingly. A rise in the input power will cause a proportional rise in the bias current of the amplifier. The detector circuit is essentially moving the loadline
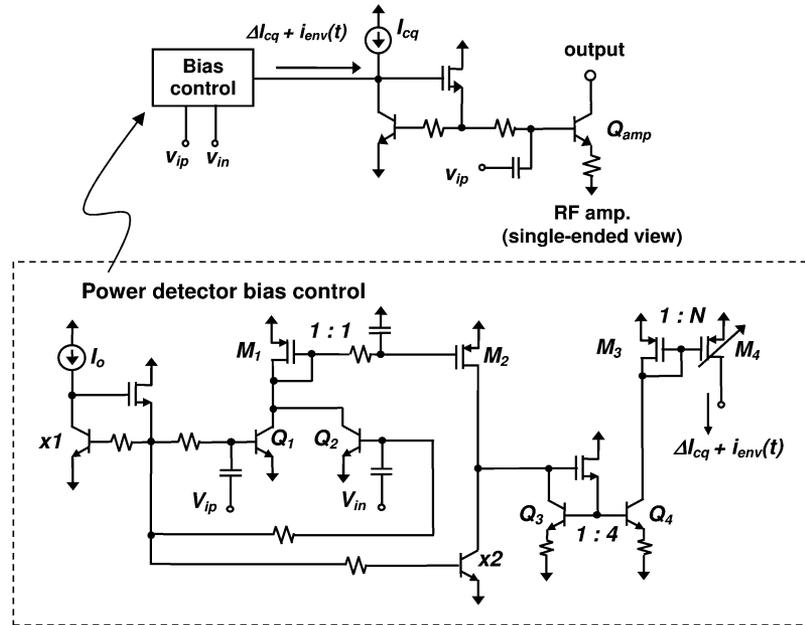
Fig. 2. Simplified schematic of the adaptively biased RF amplifier circuit.

of the amplifier as shown in Fig. 1(b) in response to the power level. As a result, large-signal distortion can be significantly reduced without increasing the quiescent power consumption.

Notice that along with the dc current boost, an envelope signal will also be superimposed, whose impact on the overall amplifier linearity is far less straightforward. This work presents a rigorous linearity analysis of a RF amplifier when injected with an envelope signal. Based on the Volterra series formulations, the study will critically examine the intricate interactions between the distortion components. The results will explain an intriguing asymmetric spectral regrowth phenomenon as observed in some experimental results, and point to an optimal design condition in which distortion components can be mutually cancelled.

This paper is organized as follows. Section II presents the Volterra series analysis on the RF amplifier with an injected envelope signal, and key third-order intermodulation distortion (IMD_3) mechanisms will be highlighted. Based on the theory, Section III offers an intuitive explanation for the asymmetrical spectral regrowth phenomenon. In addition, it illustrates the technique by which IMD_3 can be optimally cancelled by the injected envelope signal. Section IV establishes the validity of the theory by comparing it to experimental results. Conclusions will be drawn in Section V.

II. AMPLIFIER LINEARITY ANALYSIS WITH ENVELOPE SIGNAL INJECTION

Fig. 2 shows the simplified schematic of the adaptively biased RF amplifier in the WCDMA handset transmitter IC [6]. Power detection is accomplished by two bipolar devices (Q_1, Q_2) configured as common-emitter amplifiers. They are biased with low quiescent current (I_o), so that their collector currents will be "clipped" during large-signal conditions, thus raising their average (dc) collector currents above the quiescent level. The extra dc current ΔI_{cq}, which is proportional to the input power, will

be applied to the RF amplifier (Q_{amp}) through the digitally programmable $(1:N)$ bias current mirror network.

Besides the dc current boost, the adaptive bias control circuit also produces an envelope signal current as explained below. Assuming that the input RF signal is a two-tone sinusoid (of frequencies ω_1 and ω_2). When the differential collector currents of Q_1 and Q_2 are combined at the drain of transistor M_1, all odd-order terms (at ω_1, ω_2, $3\omega_1$, $3\omega_2$, $2\omega_1 \pm \omega_2$, $5\omega_1$, etc.) are cancelled, while the even-order terms (at $\omega_2 \pm \omega_1$, $2\omega_1$, $2\omega_2$, etc.) will be summed. The low-pass (single-pole) filter at the gates of M_1–M_2 will attenuate all of the remaining even-order terms except $\omega_2 - \omega_1$ (or the signal envelope) as it is the only baseband (low frequency) component.[1] This envelope signal will be fed back alongside the dc current to the main amplifier, which is given by

$$i_{\mathrm{env}}(t) = I_{\mathrm{env}} \cos[(\omega_2 - \omega_1)t + \theta_{\mathrm{env}}] \qquad (1)$$

where I_{env} and θ_{env} denote the amplitude and the phase of the envelope signal, respectively.

As a result, the bias current of the amplifier transistor (the Q_{amp} shown in Fig. 2), as well as its transconductance, are time-varying. For intermodulation calculations, this is modeled as an additional small-signal envelope signal *voltage* along with the two-tone RF signal inputs.

Volterra analysis is used to capture the frequency dependent nonlinearities, which dominate at high frequencies [7]. The equivalent nonlinear circuit is shown in Fig. 3, where Z_S, Z_E, and Z_L denote the source, emitter, and load impedances respectively. In this model, capacitance C_π and transconductance g_m are assumed to be the only nonlinear elements [8], and the transistor load impedance nonlinearity is ignored. While the load could exhibit some nonlinearity at high frequencies,

---

[1] Of course, there exist other even-order baseband components (for instance, at $2\omega_2 - 2\omega_1$) which may not get cancelled or filtered. However, since they are higher order intermodulation products with much smaller magnitudes, they can be safely neglected.

it is generally less severe as it is dominated by depletion capacitances (namely the base-collector and collector-substrate capacitances) that are less dependent on input signal (or base-emitter voltage) variations. The good agreement between theoretical, simulation and measurement results presented later appear to support our assumption.

The i–v relationship of C_π is given by

$$i = \frac{d}{dt}\left[C_C v_{be} + K_{2C} v_{be}^2 + K_{3C} v_{be}^3\right] \qquad (2)$$

where K_{2C} and K_{3C} are the second- and third-order nonlinear capacitance coefficients, and v_{be} is the base-emitter voltage. Similarly, the nonlinear collector current is given by

$$i_c = g_m v_{be} + K_{2gm} v_{be}^2 + K_{3gm} v_{be}^3 \qquad (3)$$

where K_{2gm} and K_{3gm} are the second- and third-order nonlinear transconductance coefficients. These coefficients are extracted from simulations of the bipolar transistor biased in the actual operating conditions. They will be employed to calculate the value of the nonlinear current sources $\tilde{i}_{N,C,\omega}$ and $\tilde{i}_{N,gm,\omega}$, which denote the Nth-order nonlinear capacitance and transconductance currents at frequency ω, respectively.

We limit the complexity of the nonlinearity analysis to the third-order. Higher order nonlinearities are ignored. As subsequent results indicate, this simplifying assumption is valid over the range of signal power and bias conditions that the target RF driver amplifier operates on.

In our three-tone intermodulation test, where two input frequencies are at ω_1 and ω_2, and the third (envelope) signal input is at $\omega_3 = \omega_2 - \omega_1$, we will derive the resulting distortion using the method of nonlinear currents [7]. From Fig. 3, by ignoring the nonlinear current sources, the fundamental (linear) collector and base-emitter voltages (at ω) are given by

$$v_c(\omega) = \frac{[-g_m + j\omega C_\mu(1 + g_m Z_E) - \omega^2 C_\pi C_\mu Z_E] \cdot Z_L}{D(\omega)}$$
$$\cdot v_s(\omega) \qquad (4)$$
$$v_{be}(\omega) = \frac{1 + j\omega C_\mu Z_L}{D(\omega)} \cdot v_s(\omega) \qquad (5)$$

where $D(\omega)$ is given by

$$D(\omega) = 1 - \omega^2 C_\pi C_\mu (Z_E Z_L + Z_E Z_S + Z_L Z_S)$$
$$+ g_m Z_E + j\omega$$
$$\cdot [C_\pi Z_E + C_\mu Z_L + C_\pi Z_S + C_\mu Z_S$$
$$+ C_\mu g_m (Z_E Z_L + Z_E Z_S + Z_L Z_S)]. \qquad (6)$$

Similarly, the higher order (nonlinear) collector and base-emitter voltages are found by setting the signal source (v_s) to zero. The second-order base-emitter voltage at frequency ω is found to be

$$v_{be}(\omega) = \frac{-1}{D(\omega)}$$
$$\cdot \{\tilde{i}_{2,gm,\omega}[Z_E + j\omega C_\mu(Z_L Z_S + Z_E Z_L + Z_S Z_E)]$$
$$+ \tilde{i}_{2,C,\omega}[Z_S + Z_E + j\omega C_\mu$$
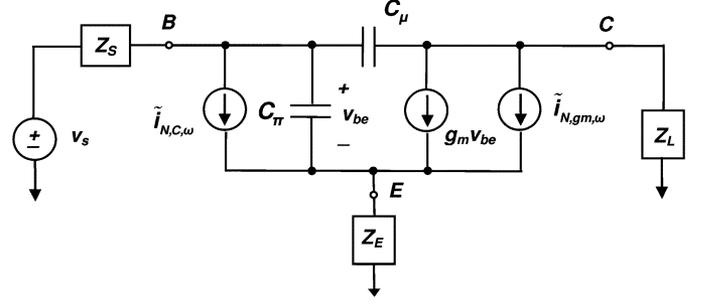$$\cdot (Z_L Z_S + Z_E Z_L + Z_S Z_E)]\}. \qquad (7)$$

Fig. 3. Nonlinear amplifier model, for Volterra analysis using the method of nonlinear currents [7]. The fundamental signals are found by setting the nonlinear current sources to zero, while higher order distortion voltages are evaluated by setting the signal source to zero.

For double frequency terms (such as $2\omega_1$), the nonlinear currents are given by [7]

$$\tilde{i}_{2,gm,2\omega} = \frac{K_{2gm}}{2} v_{be}^2(\omega)$$
$$\tilde{i}_{2,C,2\omega} = K_{2C} j\omega v_{be}^2(\omega). \qquad (8)$$

Similarly, for difference frequency terms (such as $\omega_2 - \omega_1$), the nonlinear currents are given by

$$\tilde{i}_{2,gm,\omega_a - \omega_b} = K_{2gm} v_{be}(-\omega_b) v_{be}(\omega_a)$$
$$\tilde{i}_{2,C,\omega_a - \omega_b} = K_{2C} j(\omega_a - \omega_b) v_{be}(-\omega_b) v_{be}(\omega_a). \qquad (9)$$

The third-order collector voltage can be written as

$$v_c(\omega) = \frac{-Z_L}{D(\omega)} \cdot \{\tilde{i}_{3,C,\omega}[-j\omega C_\mu Z_S + g_m(Z_E + Z_S)]$$
$$+ \tilde{i}_{3,gm,\omega}[1 + j\omega C_\mu Z_S + j\omega C_\pi(Z_E + Z_S)]\}. \qquad (10)$$

The third-order intermodulation distortion (IMD_3) currents are given by

$$\tilde{i}_{3,gm,2\omega_a - \omega_b} = K_{2gm} \cdot [① + ② + ③ + ④]$$
$$+ \frac{3K_{3gm}}{4}[⑤ + ⑥]$$
$$\tilde{i}_{3,C,2\omega_a - \omega_b} = j(2\omega_a - \omega_b) \cdot \left\{ K_{2C} \cdot [① + ② + ③ + ④] \right.$$
$$\left. + \frac{3K_{3C}}{4}[⑤ + ⑥] \right\} \qquad (11)$$

where ①–⑥ denote all possible combinations of the lower-order (fundamental and second-order) terms derived earlier that will give rise to the IMD_3 products. Specifically, for IMD_3 at $2\omega_1 - \omega_2$ (which is, say, the lower side of the channel), these six terms are

$$① = v_{be}(2\omega_1)v_{be}(-\omega_2) \qquad ② = v_{be}(\omega_2)v_{be}(-2\omega_3)$$
$$③ = v_{be}(\omega_1)v_{be}(\omega_1 - \omega_2) \qquad ④ = v_{be}(\omega_1)v_{be}(-\omega_3)$$
$$⑤ = v_{be}(-\omega_2)v_{be}^2(\omega_1) \qquad ⑥ = v_{be}(\omega_2)v_{be}^2(-\omega_3). \qquad (12)$$

By the same token, the corresponding products for the IMD_3 at $2\omega_2 - \omega_1$ (or the upper side of the channel) are

$$\mathbf{❶} = v_{be}(-\omega_1)v_{be}(2\omega_2) \qquad \mathbf{❷} = v_{be}(\omega_1)v_{be}(2\omega_3)$$
$$\mathbf{❸} = v_{be}(\omega_2)v_{be}(\omega_2 - \omega_1) \qquad \mathbf{❹} = v_{be}(\omega_2)v_{be}(\omega_3)$$
$$\mathbf{❺} = v_{be}(-\omega_1)v_{be}^2(\omega_2) \qquad \mathbf{❻} = v_{be}(\omega_1)v_{be}^2(\omega_3) \qquad (13)$$

Finally, the third-order intermodulation ratio (IMR_3) is determined by the ratio between the fundamental and the third-order collector voltage (v_c) given by (4) and (10).

Before we apply the Volterra series results to quantitatively study the amplifier linearity performance, let us consider the physical meaning of the formulations derived above. Examining (12) and (13) closely, it is found that the IMD_3 terms are generated through the following *three* different mechanisms.

1) *Cascaded second-order mixing* (①–③, and ❶-❸). In this distortion mechanism, second-order distortion components (such as the $v_{be}(2\omega_1)$ in ①) and the linear terms (such as $v_{be}(-\omega_2)$) will go through another stage of second-order nonlinearity (such as K_{2gm}) to produce a IMD3 component at $2\omega_1 - \omega_2$. This is illustrated in Fig. 4.

2) *Up-converted envelope* (④, and ❹). In this second mechanism, IMD_3 is simply created by mixing the baseband envelope signal (such as the $v_{be}(-\omega_3)$ in ④) with the RF input tone (such as $v_{be}(\omega_1)$) through the second-order nonlinearity (such as K_{2gm}). This is shown in Fig. 5.

3) *Third-order mixing* (⑤–⑥, and ❺-❻). This is the IMD_3 in its classical sense. A third-order nonlinearity (such as K_{3gm}) occurs between two linear signals. This can apply to the two RF inputs (that is, $v_{be}(-\omega_2)$ and $v_{be}(\omega_1)$ as in ⑤), or between the envelope signal and one RF input (that is, $v_{be}(\omega_2)$ and $v_{be}(-\omega_3)$ in ⑥). This is shown in Fig. 6.

To simplify the subsequent discussion without losing important insights, let us make two observations. First, notice that the products denoted by ①③⑤ (or ❶❸❺) are the conventional IMD_3 components, as they are envelope signal (ω_3) independent. In other words, these components exist regardless whether or not the envelope signal is injected into the RF amplifier. Second, among the remaining envelope-dependent terms, only ④ (or ❹) is of interest. It is because the other two terms (②⑥, or ❷❻) involve "squaring" the already small envelope input at ω_3, and can be safely ignored.

III. DISCUSSION OF THEORETICAL RESULTS

The theoretical analysis leads to an intuitive understanding of the nonlinear behavior, as well as a strategy for high-linearity high-efficiency RF amplifier design, as will be explained below.

Since the envelope-dependent mixing products ④ and ❹ will typically have different phase relationships with the conventional distortion components, their summation can result in unequal IMD_3 amplitudes at $2\omega_1 - \omega_2$ and $2\omega_2 - \omega_1$. This scenario is graphically demonstrated in Fig. 7, where the nonlinear current components are represented by vectors to highlight their interactions. In this example, the angle between
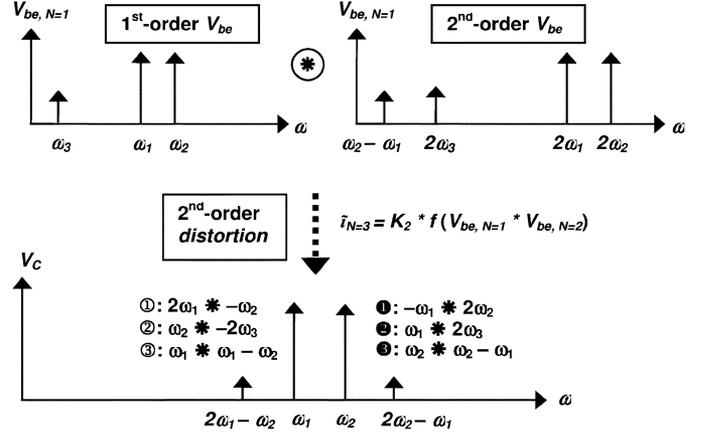

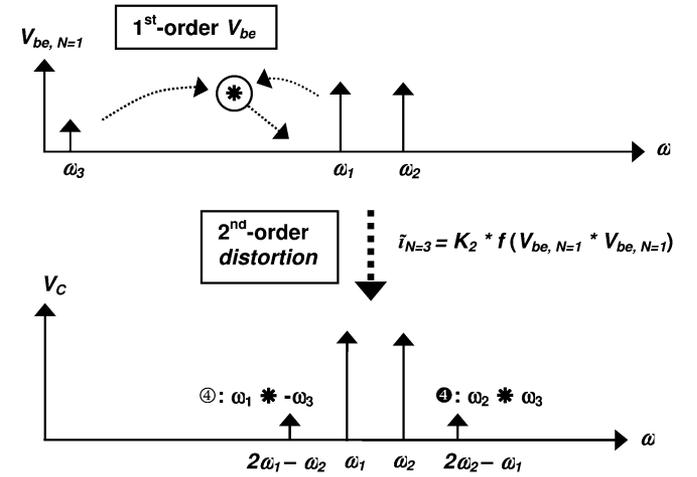Fig. 4. First mechanism for IMD_3 generation: cascaded second-order mixing.

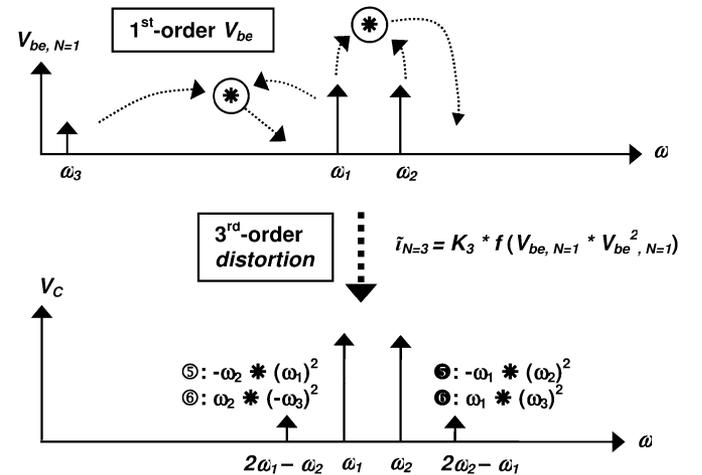Fig. 5. Second mechanism for IMD_3 generation: up-converted envelope.

Fig. 6. Third mechanism for IMD_3 generation: third-order mixing.

vectors ❹ and $\sum[\mathbf{❶\,❸\,❺}]$ is less than that between ④ and $\sum[①③⑤]$ (i.e., $\theta_1 < \theta_2$). As a result, their resultant vectors will exhibit different magnitudes. So, the IMD_3 at $2\omega_2 - \omega_1$ will be higher than that at $2\omega_1 - \omega_2$. It shows that asymmetric spectral regrowth is possible despite the fact that the individual distortion components are equal in magnitude at both frequencies.
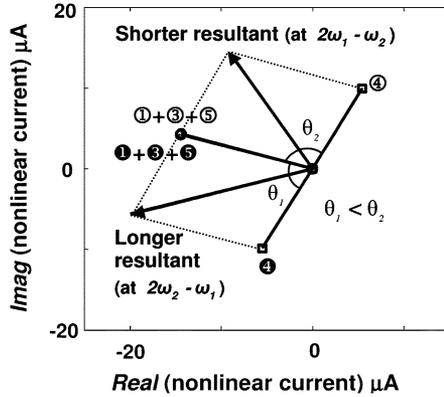
Fig. 7. Vector diagram illustrating the cause of IMD_3 asymmetry. Vectors ④ and ❹ represent the injected envelope signal. Note that the two resulting IMD vectors will have different amplitudes depending on the phase of the envelope.
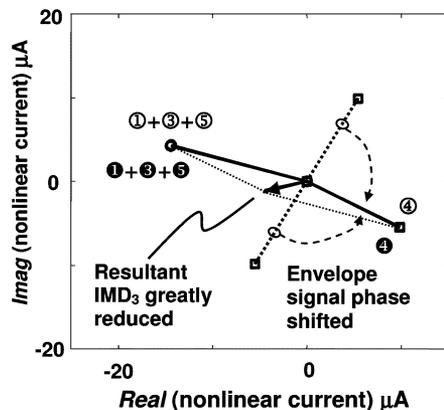

Fig. 8. Vector diagram showing optimal IMD_3 cancellation. Note that the injected envelope signal cancels the third-order components when its phase and amplitude are optimized.

The vector diagram also points to the fact that if the injected envelope signal is too strong, vectors ④ and ❹ will dominate the final IMD_3 resultant vector. That is, the "second-order" product due to the envelope signal at $\omega_2 + \omega_3 = 2\omega_2 - \omega_1$ would mask the true "third-order" intermodulation of the amplifier at the same frequency. The detector circuit is causing worse spectral regrowth than if it is absent, which is highly undesirable.

Nevertheless, the vector analysis also leads to a method for IMD_3 cancellation. It is straightforward to show that if the envelope signal is phase-shifted (with respect to the input RF signals), vectors ④ and ❹ will always rotate in opposite direction by the same angle: if one vector moves clockwise, the other will travel counter-clockwise. If these vectors can be simultaneously rotated to be at $180°$ opposite to the vectors of $\sum[①③⑤]$ and $\sum[❶❸❺]$, and they are of equal magnitude, the IMD_3 at both frequencies will be greatly reduced.

The above scenario is realized in Fig. 8. We introduce a phase shift (of $+90°$) to the envelope signal when it is injected back to the main amplifier. As a result, both envelope-dependent non-linear current vectors move to align themselves $\sim180°$ opposite to the fixed IMD_3 components. The resultant IMD_3 vectors at both $2\omega_1 - \omega_2$ and $2\omega_2 - \omega_1$ frequencies are substantially reduced.

The effect of the phase of the envelope signal on intermodulation distortion is shown in Fig. 9. The circuit of Fig. 2 was
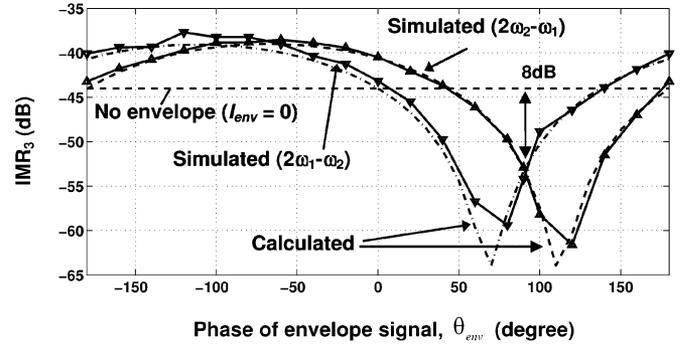

Fig. 9. Comparison between calculation and simulation of IMD asymmetry with varying envelope injection phase. Maximum IMR_3 cancellation is achieved when the envelope signal is injected with the optimal phase relative to the RF inputs.

simulated at the maximum power level, and an envelope signal of fixed amplitude and arbitrary phase is injected. The two-tone simulation results are compared with the theoretical predictions, and excellent agreement is observed. The simulation verifies our intuition that optimal IMD cancellation will result at a particular envelope signal amplitude and phase angle. In this case, IMD at $2\omega_2 - \omega_1$ and $2\omega_1 - \omega_2$ show simultaneous improvement of 8 dB.

Since the envelope detector circuit is very low-power and it operates at baseband, the distortion cancellation technique has good potential for achieving both high-linearity *and* high-efficiency to meet the stringent requirements for modern communication applications. Intuitively speaking, the approach is sound over process and temperature variations. It is because the injected envelope signal (from the detector circuit) should track the main amplifier distortion components as they are generated by matching devices which reside on the same chip. However, further investigation (such as running skewed wafers) is required to fully characterize the distortion cancellation technique's viability across process corners.

IV. MEASUREMENT RESULTS

A WCDMA RF amplifier incorporating the envelope detection circuit of Fig. 2 has been fabricated in a 0.25 μm SiGe BiCMOS process [9]. The chip (single-ended) measures 1.75×0.7 mm^2 (including pads) as shown in Fig. 10. The amplifier has 16.5 dB gain with 4.5 mA (with 2.7-V supply) quiescent current consumption. The power detector bias control improves the output $P_{1\mathrm{dB}}$ by 3.5 dB to 9.7 dBm when it is enabled. A more detailed discussion on the circuit design and the performance characterization can be found in [10]. Here, we focus on the experimental results pertaining to the detection circuit and the effects of envelope injection.

Fig. 11 displays the measured current consumption of the RF amplifier versus the output power. Additional current is provided when the detector is enabled (with current mirror ratio increased from 2 $\times$ to 4 $\times$). The detector circuit provides 25% higher bias current at the 1-dB compression point. Assuming a typical CDMA signal probability distribution, the amplifier with the detector bias control (4 $\times$ mirror ratio) produces an average efficiency of 2.0%. It should be compared to an average efficiency of 1.4% for a standard-biased (Class A) amplifier for similar linearity performance.
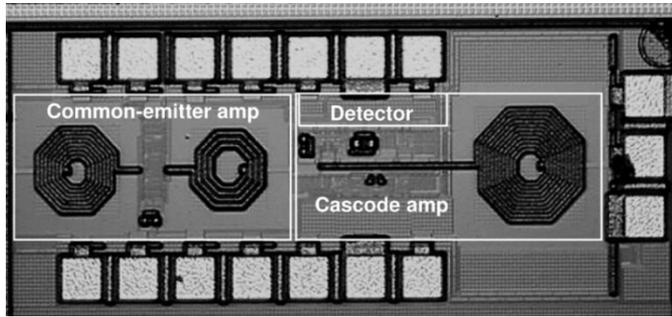
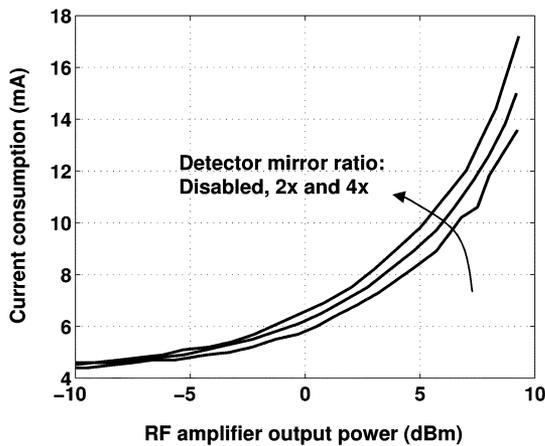Fig. 10.   Microphotograph of the RF amplifier chip.

Fig. 11.   Measured current consumption of the RF amplifier versus output power levels.
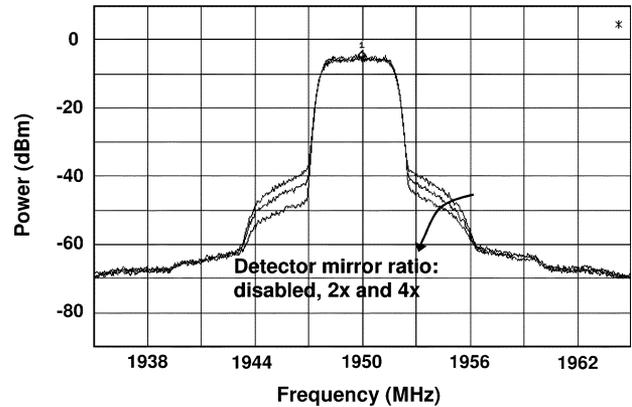

Fig. 12.   Measured RF amplifier output spectrum. While the envelope detector circuit improves the ACPR, spectral regrowth asymmetry is observed.
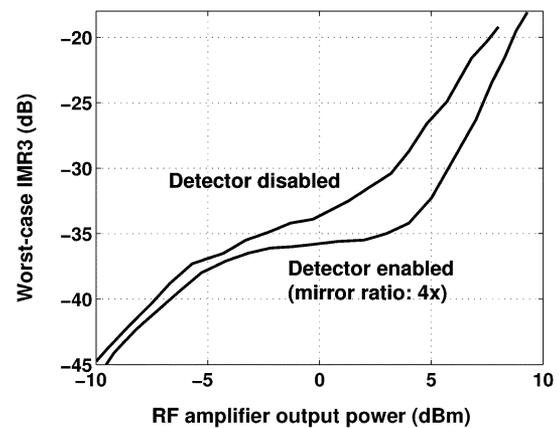

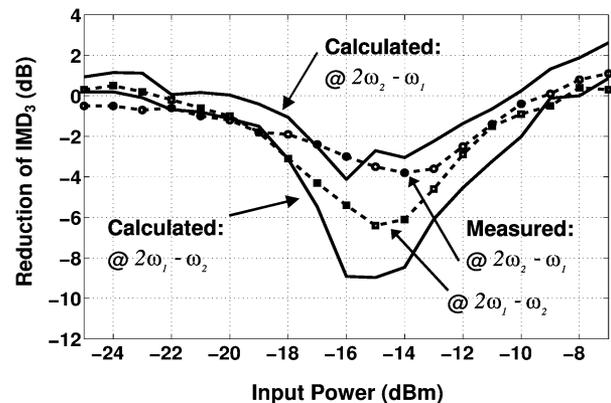Fig. 13.   Measured RF amplifier IMR_3 versus output power levels.

Fig. 14. IMD_3 reduction versus input when the envelope detector is enabled (mirror ratio: $4\times$). Good agreement is observed between the calculation and measured results, thus confirming the Volterra series analysis.

Fig. 12 shows the measured output spectrum at 0.5 dBm (single-ended) output power. The adjacent channel regrowth at 5 MHz offset is caused by the third-order IMD. It is reduced when the detector circuit is enabled. The adjacent channel power ratio (ACPR) is improved by 6 dB to −43 dBc.[2] As is evident in the figure, the ACPR improvement due to the detector circuit is *asymmetrical*. Better ACPR results are observed at the lower-side of the channel. This asymmetry is mainly caused by the envelope signal injection as explained in the previous Section. In the current chip implementation, the phase of the injected envelope is approximately $+40°$ with respect to the RF input signals, which, according to Fig. 9, should give rise to enhanced IMD_3 rejection at the lower side.

Fig. 13 presents the measured amplifier third-order intermodulation distortion results. Two sinusoidal signals at 1.9475 and 1.9525 GHz are applied. The test is conducted for a wide range of input powers up to the input 1-dB compression point. Obviously, IMR_3 is improved when the detector circuit is enabled and set to a current mirroring ratio of $4\times$. Fig. 14 shows the measured IMD_3 improvement at the upper and the lower side. The measured data are compared to the Volterra series calculations, and very good agreement is obtained. This establishes the validity of the theoretical analysis conducted in Section II.

V. CONCLUSION

The effects of envelope signal injection on RF amplifier linearity have been rigorously studied by Volterra series analysis. It highlights the three underlying physical mechanisms by which third-order intermodulation distortions are generated. The study provides intuitive explanation to an intriguing asymmetrical spectral regrowth phenomenon. It also points to a technique to mutually cancel the inherent distortion components of the (low-power) RF amplifier, so that the dual (conflicting) goals

[2]The detector circuit is designed to produce good ACPR enhancement around the maximum average output power (of 0.5 dBm), which is approximately 9 dB below the 1-dB compression point. The 9-dB difference is a typical design margin to account for the high peak-to-average-power-ratio (PAR) of WCDMA signal to avoid amplifier clipping.

of high linearity and high efficiency can be simultaneously achieved. Very good agreement is observed between the theory, the simulated results, and the measured results.

The envelope detector circuit is compact and low-power. Moreover, the envelope signal generation, feedback and injection all take place at baseband frequencies where the signal processing is relatively straightforward. Therefore, the linearity enhancement technique demonstrates good potential to meet the RF amplifier design challenges for future wireless applications. One possible design target would be power amplifiers with very high output levels, which would be the subject for future investigation.
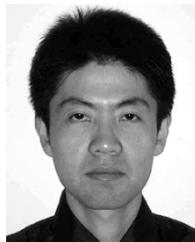
References

[1] *3GPP Standard*, TS 25.101 (V5.3.0), 2002.

[2] M. van der Heijden, M. Spirito, M. Pelk, L. deVreede, and J. Burghartz, "On the optimum biasing and out-of-band-terminations of linear and power efficient class-AB bipolar amplifiers," in *Proc. IEEE BCTM*, Sep. 2004, pp. 44–47.

[3] J. Groe and L. Larson, *CDMA Mobile Radio Design*. Norwood, MA: Artech House, 2000.

[4] E. Taniguchi, K. Maeda, T. Ikushima, K. Sadahiro, K. Itoh, N. Suematsu, and T. Takgai, "Dual bias feed SiGe HBT low noise linear amplifier," in *IEEE MTT-S Int. Microwave Symp. Dig.*, May 2001, pp. 285–288.

[5] S. Shinjo, K. Mori, H. Joba, N. Suematsu, and T. Takagi, "Low quiescent current SiGe HBT driver amplifier having self base bias control circuit," *IEICE Trans. Electron.*, vol. E85-C, no. 7, pp. 1404–1411, Jul. 2002.

[6] V. Leung, L. Larson, and P. Gudem, "Digital-IF WCDMA handset transmitter IC in 0.25 μm SiGe BiCMOS," in *IEEE Int. Solid-State Circuits Dig. Tech. Papers*, Feb. 2004, pp. 182–183.

[7] P. Wambacq and W. Sansen, *Distortion Analysis of Analog Integrated Circuits*. Boston, MA: Kluwer, 1998, pp. 137–156.

[8] S. A. Maas, *Nonlinear Microwave Circuits*. Norwood, MA: Artech House, 1998, pp. 190–207.

[9] IBM 6HP BiCMOS Process. [Online]. Available: http://www-3.ibm.com/chips/techlib/techlib.nsf/products/BiCMOS_6HP

[10] V. Leung, L. Larson, and P. Gudem, "Digital-IF WCDMA handset transmitter IC in 0.25-μm SiGe BiCMOS," *IEEE J. Solid-State Circuits*, vol. 39, no. 12, pp. 2215–2225, Dec. 2004.

Junxiong Deng (S'02) received the B.S. degree in electrical engineering from Southeast University, Nanjing, China, in 1997, the M.S. degree in electrical engineering from the University of California at San Diego (UCSD), La Jolla, in 2002, and is currently working toward the Ph.D. degree at UCSD.

His research concerns wireless RF circuit design, particularly high-efficiency and high-linearity power amplifiers for advanced wireless communication systems.

Prasad S. Gudem received the Ph.D. degree in electrical and computer engineering from the University of Waterloo, Waterloo, Canada, in 1996. His doctoral research concerned the modeling and numerical simulation of amorphous silicon devices.

After a brief time with Mitel Semiconductors, Kanata, Canada, he joined Cadence Design Systems, San Diego, CA, where he was involved with semiconductor-device modeling for analog and RF applications. In 2000, he joined the IBM T. J. Watson Research Center, Yorktown Heights, NY, where he was involved with RF integrated circuit design for WCDMA applications using IBM's SiGe technology. He recently joined Qualcomm, San Diego, CA, where he is leading the development of zero IF diversity receiver chips. He is also co-advising several graduate students in their Ph.D. research in the Department of Electrical and Computer Engineering at the University of California at San Diego (UCSD).

Dr. Gudem received the Graduate Teaching Award for the 2001–2002 academic year in recognition of his outstanding teaching of the popular ECE265 course sequence (Communication Circuit Design: I, II & III).

Vincent W. Leung (M'97) received the B.Eng. and M.Eng. degrees in electrical engineering in 1995 and 1998, both from McGill University, Montreal, Canada, and the Ph.D. degree in electrical engineering from the University of California at San Diego, La Jolla, in 2004.

From 1997 to 2000, he was at Analog Devices, Somerset, NJ, where he was engaged in the design of xDSL analog IC chips. He joined IBM T. J. Watson Research Center, Yorktown Heights, NY, in 2004. He is the coauthor of the book *Design and Analysis of Integrator-Based Log-Domain Filter* (Boston, MA: Kluwer Academic, 2000), and holds one U.S. patent.

Dr. Leung was the recipient of the Second Prize in SRC's SiGe Design Contest for his doctorate research.

Lawrence E. Larson (M'82–SM'90–F'00) received the B.S. degree in electrical engineering in 1979 and the M.Eng. degree in 1980, both from Cornell University, Ithaca, NY. He received the Ph.D. degree in electrical engineering from the University of California at Los Angeles in 1986.

From 1980 to 1996, he was with Hughes Research Laboratories, Malibu, CA, where he directed the development of high-frequency microelectronics in GaAs, InP, and Si/SiGe and MEMS technologies. He joined the faculty at the University of California at San Diego (UCSD) in 1996, where he is the inaugural holder of the Communications Industry Chair. He is currently Director of the UCSD Center for Wireless Communications. During the 2000–2001 academic year, he was on leave at IBM Research, San Diego, CA, where he directed the development of RFICs for 3G applications. He has published over 200 papers, co-authored three books, and has received 27 U.S. patents.

Dr. Larson was the recipient of the 1995 Hughes Electronics Sector Patent Award for his work on RF MEMs, co-recipient of the 1996 Lawrence A. Hyland Patent Award of Hughes Electronics for his work on low-noise millimeter-wave HEMTs, and the 1999 IBM Microelectronics Excellence Award for his work in Si/SiGe HBT technology.